Relationship between Craze Microstructure and Molecular Entanglements in Glassy Polymers. 1

Larry L. Berger

E. I. du Pont de Nemours and Company, Inc., Central Research and Development Department, Experimental Station, Wilmington, Delaware 19898.
Received October 4, 1988; Revised Manuscript Received January 12, 1989

ABSTRACT: Low-angle electron diffraction was used to characterize the microstructure of crazes grown in a series of glassy polymers, spanning a wide range in molecular entanglement density ν_e. Specifically, the mean craze fibril diameter D, the mean craze fibril spacing D_0, and the orientation φ of the fibril axis with respect to the tensile axis were determined for crazes grown at a constant rate and homologous temperature ($T - T_g = -75$ °C). Both D and D_0 were observed to increase modestly with increasing ν_e. In addition φ was found to increase almost linearly with ν_e; this increase reflects the increased contribution of cross-tie fibrils in controlling the craze microstructure in high-ν_e networks. The measured dependence of the craze microstructural parameters on ν_e is found to be in satisfactory agreement with the meniscus instability model of craze growth, which predicts that the scale of fibrillation is controlled by ν_e.

Introduction

A host of recent experiments on thin films of polymer glasses have unambiguously demonstrated the importance of the molecular network in governing the crazing stress, mechanism of plastic deformation (either crazing or shear), and the strain hardening behavior in these materials.[1-7] In short, it was found that polymers having a high entanglement density $\nu_e > 11.0 \times 10^{25}$ strands/m^3 (where $\nu_e = \rho N_a/M_e$, ρ = specific density, N_a = Avogadro's number, and M_e is the entanglement molecular weight determined from the short-term elastic modulus of the rubbery plateau) and concomitantly a short entanglement length l_e (=length of chain between entanglement points) were ductile and deformed by shear yielding. Typically these materials exhibit strains up to 25% and more prior to macroscopic fracture. In contrast, when subjected to a tensile strain, polymers with a low ν_e ($<4 \times 10^{25}$ strands/m^3) and hence large l_e were found to be brittle and deform exclusively by crazing. For polymers with intermediate values of ν_e (and thus l_e) competition between shear deformation and crazing, in the same film, was observed.

In addition, the value of the network extension ratio (determined by optical densitometry of electron image plates) within the craze λ_{craze} or shear deformation zone (DZ) λ_{DZ} was found to correlate with the maximum theoretical extension ratio of an entangled strand in the glassy network λ_{Net}.[2,3] Here $\lambda_{Net} \cong 3^{1/2} l_e/d$, where d = root-mean-squared end-to-end distance of an entangled polymer strand with mass M_e. Since l_e scales as ν_e^{-1} and d as $\nu_e^{-1/2}$, then λ_{Net} scales as $\nu_e^{-1/2}$. Invariably for polymer glasses it was found that λ_{craze} ($\sim 0.5\lambda_{Net}$) > λ_{DZ} ($\sim 0.3\lambda_{Net}$), a result that was rationalized by considering the type(s) of modification that the molecular network must undergo during the formation of either craze of DZ. Through a series of experiments[4,8,9] it was demonstrated that the production of the inherently fine fibril and void microstructure within the craze requires a loss of entangled strands from the polymer network (through either chain scission or chain disentanglement processes) whereas the formation of a shear DZ involves only a localized micronecking of the glass. For crazes, this decrease in polymer strand density is believed to produce $\lambda_{craze} > \lambda_{DZ}$; consequently crazes are inherently more brittle than DZs.

Recently the development of low-angle electron diffraction LAED methods, for the characterization of the craze microstructure,[10-14] has shed important insight on both the processes of craze fibril formation and craze fibril breakdown. (This latter topic will be addressed in a subsequent publication.) In particular LAED has proven ideally suited for studying the microstructure of individual crazes grown in well-characterized samples (e.g., monodisperse polymers and polymers having a uniquely specified topology). The advantage of this technique vis à vis small-angle X-ray scattering (SAXS)[15-17] is 2-fold: LAED requires only a small quantity of polymer and, with the use of a selected-area aperture in the TEM, allows the properties of a single craze to be examined. This latter point is particularly important in that a bright-field electron micrograph in conjunction with a selected-area diffraction pattern permits a detailed description of the craze microstructure to be obtained. With LAED one can determine the mean craze fibril diameter D, the mean craze fibril spacing D_0, and the orientation φ of the craze fibrils with respect to the tensile axis. In turn the scales of D_0 and φ are believed to control the craze fibril stability.[5,6,18]

Clearly it is desirable to have information on the variation of these parameters for crazes formed, under the same conditions, in polymer glasses with inherently different entanglement densities. However, to date, only very limited information is available. In this paper we report on the results of a systematic study of the craze microstructure produced in a series of glassy homopolymers, copolymers, and fully compatible blends spanning a wide range of ν_e. In addition some recent models of craze growth,[19,20] which predict that the scale of fibrillation in the craze is governed by ν_e, will be tested.

Experimental Section

The following polymers spanning a range of entanglement densities were used in this study: (1) two monodisperse poly(methyl methacrylate)s (PMMA) samples having a weight-average molecular weight M_w (and molecular weight distribution M_w/M_n) = 480K (1.09) and 2600K (1.3), respectively; (2) two monodisperse poly(α-methylstyrene)s (PαMS), purchased from the Pressure Chemical Co., having a weight-average molecular weight M_w (and M_w/M_n) = 425K (1.1) and 641K (1.1), respectively; (3) a random copolymer of poly(styrene–acrylonitrile) (PSAN), obtained from Polysciences Inc., consisting of 0.25 AN with M_w = 160K; (4) two series of fully compatible blends, each comprised of a narrow molecular weight polystyrene (PS), obtained from the Pressure Chemical Co., and a polydisperse poly(2,6-dimethyl-1,4-phenylene oxide) (PPO), obtained from Scientific Polymer Products Inc. The first blend type consisted of a high molecular weight PS, with M_w = 90K and M_w/M_n = 1.06, blended with PPO, having M_w = 244K and M_w/M_n = 5. In this case blends consisting of PPO with weight fraction χ = 0, 0.2, and 0.4 were prepared. The second blend type consisted of a low molecular weight PS, having M_w

0024-9297/89/2222-3162$01.50/0

Table I

polymer	T_g, °C	$10^{-25}\nu_e$, strands/m^3	λ_{craze}
PαMS (M_w = 425 K)	175	4.8	3.5
(M_w = 641K)			
PSAN (M_w = 160K)	105	5.6	2.7
PMMA (M_w = 2600K)	110	7.8	2.0[a]
(M_w = 480K)			
PPO–PS (M_w = 90K)			
χ = 0	100	3.3[b]	4.0[a]
χ = 0.2	123	5.4[b]	3.6[a]
χ = 0.4	139	7.6[b]	3.3[a]
PPO–PS (M_w = 4K)			
χ = 0.6	147	5.3[b]	3.5[a]
χ = 0.7	160	7.3[b]	3.3[a]

[a] From ref 2. [b] Determined from M_e values given in ref 20.

= 4K and M_w/M_n = 1.06, blended with the same PPO, with weight fraction χ = 0.6, and 0.7.

Dilute solutions of each PMMA, PαMS, and PSAN in methylene chloride and blends of PS–PPO in chloroform were prepared and filtered through a 10-μm pore size filter. Thin films of all of the above polymers were produced by drawing carefully cleaned glass slides from the appropriate solutions at a constant rate. By adjusting the viscosity of the respective solutions, films having a thickness of ~0.6 μm were prepared. These films were floated off onto the surface of a water bath and picked up on well-annealed copper grids, the bars of which were previously coated with the same polymer.[21] After drying, the films were briefly plasticized by exposure to the vapor of the solvent; this procedure ensures good adhesion between the film and the grid bars. Subsequently all of the samples were physically aged at 90 °C, under vacuum, for 15 h prior to straining.

The glass transition temperature T_g for the various polymers and polymer blends, determined by using a Mettler TA3000 differential scanning calorimeter (DSC) at a heating rate of 10 °C/min, is given in column 1 of Table I. As produced, all of the polymers examined were amorphous and glassy as indicated.

The samples were placed in a micromechanical rig coupled to a reflected light microscope and enclosed in a constant-temperature environment. All of the samples were deformed at $T - T_g$ = −75 °C and at a constant strain rate of 4.0×10^{-6} s^{-1} up to a tensile strain of 0.03–0.05. Where appropriate, suitable individual film squares were isolated from the grid and examined in the transmission electron microscope (TEM).

Low-angle electron diffraction was performed by using a JEOL 2000EX TEM fitted with a LaB_6 filament and operated at 200 kV in the high-dispersion diffraction mode. A spot size of 7 and a camera length of 62.0 m, calibrated by using a carbon waffle grating with 463-nm spacing, was employed. The strongly coherent nature of the primary beam was evident since up to the tenth order of diffraction from the calibration grating was recorded. A single wide craze was placed within a 20-μm-diameter objective aperture, and the diffraction pattern was collected from this region. In all cases the minimum electron exposure needed to produce the LAED pattern was used. In particular for PMMA, which is a known positive electron resist, special care was required to minimize the electron beam damage. (In this case, the alignment of the TEM in the high-dispersion diffraction mode was carried out, and then a selected craze was introduced into the aperture; only afterward was a limited bright-field examination of the sample performed.)

A LKB-XL laser optical densitometer with a stepping distance corresponding to 100 μm × 100 μm aperture was used to scan, two-dimensionally, the LAED patterns. The optical density on the electron image plates was converted to electron intensity and summed along (the y axis) a direction that is parallel to the projection of the primary fibril axis and is normal to the craze/bulk interfaces (which lie along the x axis). From this summation, which corresponds to slit-collimated SAXS, a plot of scattered intensity $i(s_x)$, where $|s_x|$ is the scattering vector = $2\theta/\lambda$, 2θ is the scattering angle, and λ is the electron wave length, versus s_x is generated. This plot exhibits a peak in intensity at $s_x = s_{max}$ from which, using Bragg's law, a rough measure the craze fibril spacing $D_0 \sim 1/s_{max}$ may be obtained. As will be described later, a more precise value of D_0 may be obtained from the fibril diameter D, which in turn may be determined from a Porod analysis of the high-angle portion of the scattering curve.

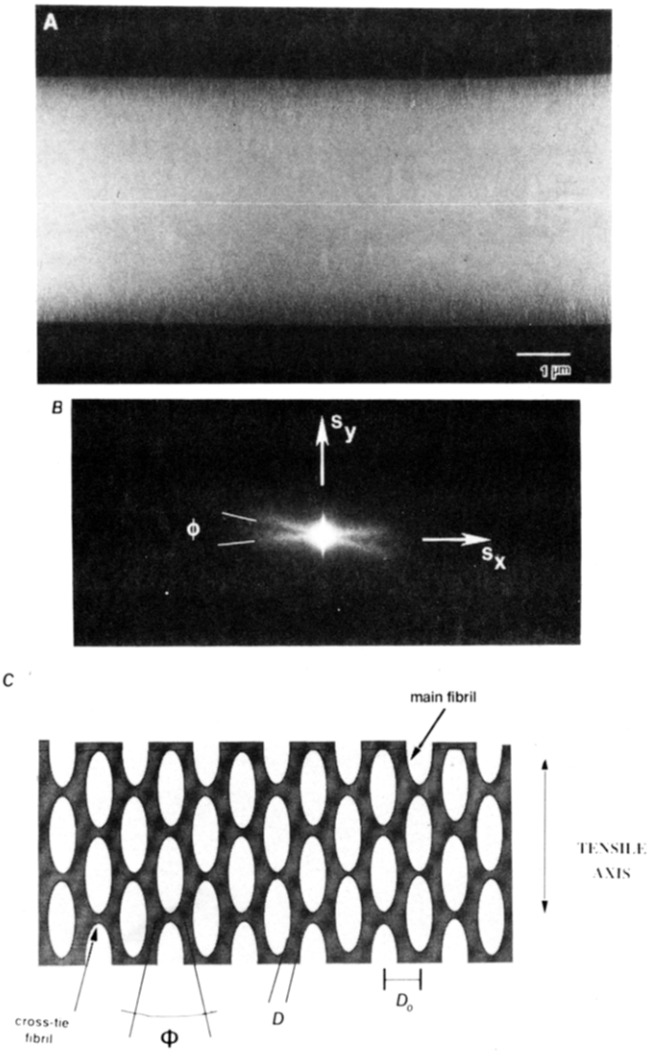

Figure 1. Bright-field TEM image of craze (A) formed in PMMA and its corresponding low-angle electron diffraction pattern (B); an idealized representation of the craze microstructure (C).

Results

Presented in Figure 1A,B are a bright-field TEM micrograph of a craze grown in a PMMA sample and its corresponding LAED pattern. This sample was deformed at 35 °C and at a slow strain rate of 4.0×10^{-6} s^{-1}. The strongly overlapping nature of the fibrillar structure, whose primary direction lies along the tensile axis, is evident in Figure 1A. The LAED pattern produced from this microstructure reveals several notable features: First the prominent horizontal streak of scattered intensity, on both sides of the forward scattered beam, lying along the s_x direction (normal to the fibril axis) arises from the small-angle diffraction of the cylindrical fibrils within the craze. Also evident is a fine vertical streak, lying along the s_y direction, that is produced by the refraction of electrons at the craze-bulk interface.[10] Since this vertical streak does not provide information on the periodicity of the craze microstructure[22] and does not contribute to the scattered intensity, in what follows we will neglect this intensity and focus our attention on the horizontal streak.

Depicted in Figure 1C, based on TEM images, is an idealized representation of the craze microstructure which is useful in identifying several features of the craze that will be discussed later. Both the mean craze fibril diameter D and craze fibril spacing D_0 (the distance between

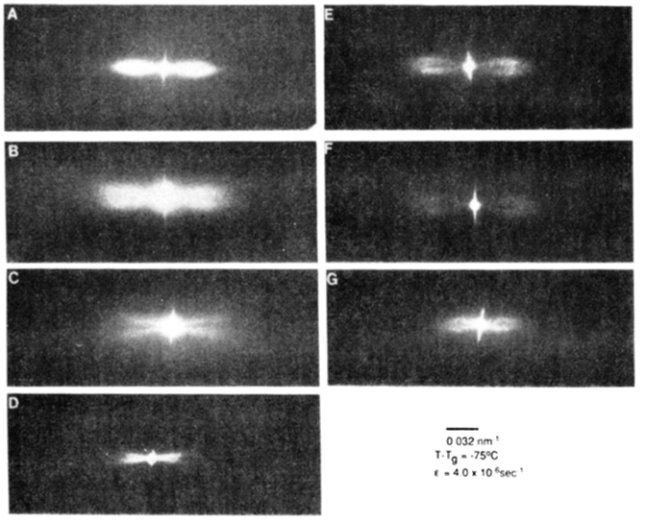

Figure 2. LAED patterns recorded from crazes formed at $T - T_g = -75$ °C in PαMS (A), PSAN (B), PMMA (C), PPO–PS (M_w = 90K) with $\chi = 0$ (D), 0.2 (E), 0.4 (F), and PPO–PS (M_w = 4K) with $\chi = 0.7$ (G).

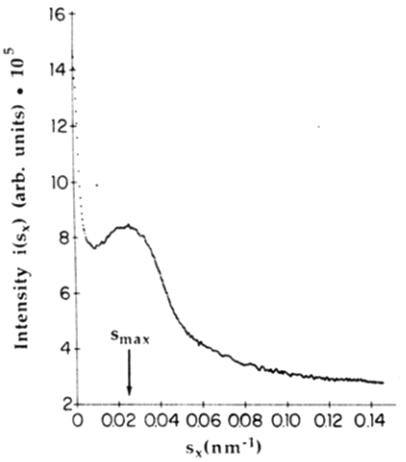

Figure 3. Plot of the slit-smeared scattered intensity $i(s_x)$ (summed along a direction parallel to the fibril axis) versus scattering vector s_x.

nearest-neighbor fibrils) are illustrated. In addition as indicated the principal fibril direction, although roughly parallel to the tensile axis, exhibits two preferred orientations, at an angle $\pm(\varphi/2)°$ from the tensile axis.[13,14] The existence of this orientation is apparent from the LAED pattern in Figure 1B, which clearly shows that each lobe of the horizontal streak exhibits a splaying (symmetric about the s_x direction) that results from two principal fibril axis orientations. This splitting produces a diffraction pattern that has a "dragonfly wing" appearance. As illustrated in Figure 1B,C, the extent of this splaying may be quantitatively characterized by an angle φ (the method by which φ is determined will be given below).

LAED patterns recorded from crazes grown, at a constant $T - T_g = -75$ °C, in samples of PαMS (M_w = 641K), PSAN (M_w = 160K), PMMA (M_w = 480K), and blends of PPO–PS (M_w = 90K) with $\chi = 0$, 0.2, and 0.4 and PPO–PS (M_w = 4K) with $\chi = 0.7$ are shown in Figure 2. An examination of these patterns reveals important qualitative differences in both the length of the scattered (horizontal) streak and the degree of splaying. A plot of the slit-smeared intensity $i(s_x)$ versus s_x for the LAED pattern shown in Figure 2A is presented in Figure 3. As indicated, this curve exhibits a well-defined peak maximum in intensity at $s_x = s_{max}$. From Bragg's law, this peak position (i.e., $1/s_{max}$) yields a semiquantitative measure of the craze

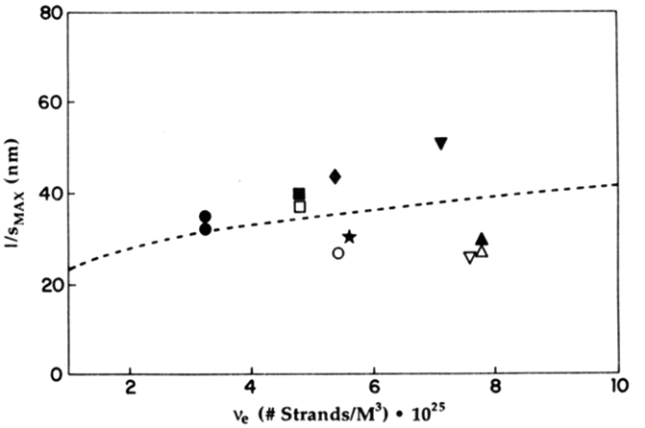

Figure 4. Plot of $1/s_{max}$ versus ν_e (entanglement density) for crazes grown, at $T - T_g = -75$ °C, in the following samples: PαMS (425K (□) and 641K (■)), PSAN (★), PMMA (480K (△) and 2600K (▲)), PPO–PS (90K) with $\chi = 0$ (●), 0.2 (○), and 0.4 (▽) and PPO–PS (4K) with $\chi = 0.6$ (◆) and 0.7 (▼).

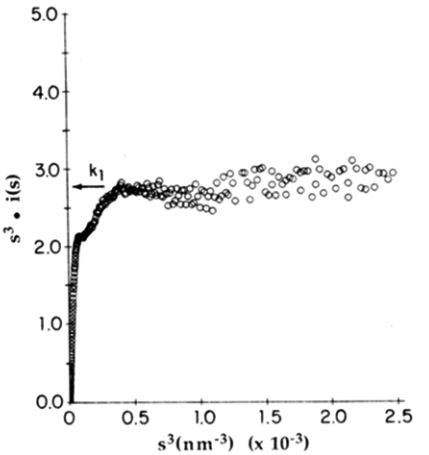

Figure 5. Background-corrected Porod plot for the curve shown in Figure 3. The value of the Porod constant k_1 ($=is^3$) is indicated.

fibril spacing (≈30 nm). Similar traces were performed for all of the LAED patterns displayed in Figure 2 from which the peak position was determined for each curve. A plot of $1/s_{max}$ versus ν_e (entanglement density), listed in column 2 of Table I, for all of the homopolymers and polymer blends examined in displayed in Figure 4. Despite the scatter in the data, it can be seen that $1/s_{max}$ increases slowly with increasing ν_e.

The value of the mean craze fibril diameter D may be obtained from an analysis of the high-angle portion of the scattering curve, which obeys Porod's law,[10-12,23] i.e.

$$k_1 = is^3 \tag{1}$$

where k_1 is the so-called Porod constant, whose value is proportional to the specific surface area of the craze fibrils. In practice k_1 is determined by extrapolating the plot of is^3 versus s^3 to $s = 0$ (after subtracting the background intensity far from the beam stop). Displayed in Figure 5 is a background-corrected Porod plot for the curve shown in Figure 3. It can be seen that this curve exhibits a nearly constant value of is^3 at high angles from which k_1 may be determined. The average value of D may be computed from the following expression:

$$D = \langle D^2 \rangle / \langle D \rangle = Q/[k_1 \pi^3 (1 - v_f)] \tag{2}$$

where Q is the small-angle scattering invariant defined as[24]

$$Q = 2\pi \int_0^\infty si(s)\, ds \tag{3}$$

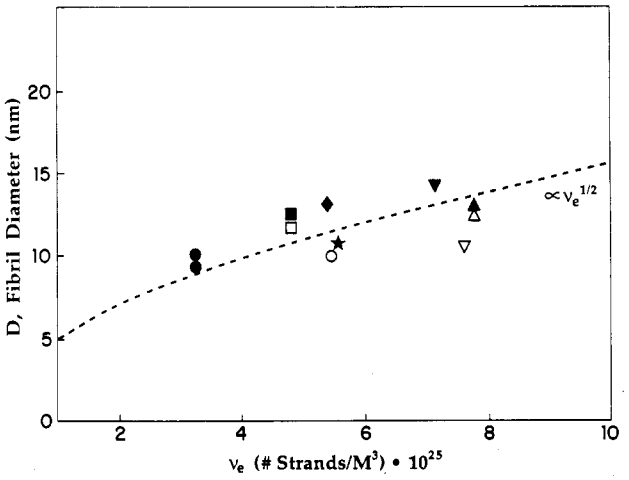

Figure 6. Plot of D versus ν_e for crazes grown, at $T - T_g = -75$ °C, in the following samples: PαMS (425K (□) and 641K (■)), PSAN (★), PMMA (480K (△) and 2600K (▲)), PPO–PS (90K) with $\chi = 0$ (●), 0.2 (○), and 0.4 (▽), and PPO–PS (4K) with $\chi = 0.6$ (◆) and 0.7 (▼). The dashed line ($\propto \nu_e^{1/2}$) corresponds to the prediction based on the meniscus instability model.

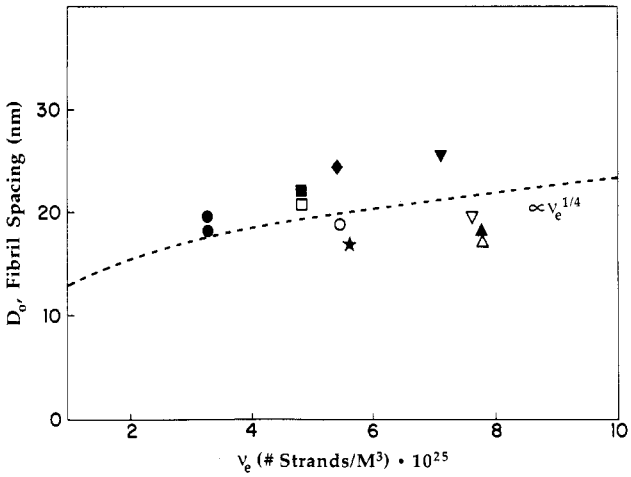

Figure 7. Plot of D_0 versus ν_e for crazes grown, at $T - T_g = -75$ °C, in the following samples: PαMS (425K (□) and 641K (■)), PSAN (★), PMMA (480K (△) and 2600K (▲)), PPO–PS (90K) with $\chi = 0$ (●), 0.2 (○), and 0.4 (▽), and PPO–PS (4K) with $\chi = 0.6$ (◆) and 0.7 (▼). The dashed line ($\propto \nu_e^{1/4}$) corresponds to the prediction based on the meniscus instability model.

and v_f ($=1/\lambda_{craze}$), listed in column 3 of Table I, is the volume fraction of polymer within the craze.

A plot of D versus ν_e, at $T - T_g = -75$ °C, for the various polymers examined is shown in Figure 6. From this plot it is apparent that D increases slowly with increasing ν_e from $D = 9$ nm in PS to $D \sim 14.5$ nm in the blend consisting of PPO–PS (4K) with $\chi = 0.7$. In addition, shown in this plot are the values of D determined for each of two different molecular weight samples of PMMA and PαMS: The filled and open triangles correspond to PMMA of molecular weight 2600K and 480K, respectively, and the filled and open squares correspond to PαMS of molecular weight 641K and 425K, respectively. As illustrated within the experimental uncertainty, at $T - T_g = -75$ °C, D exhibits no significant molecular weight dependence.

Since the semiquantitative measure of the craze fibril spacing $1/s_{max}$ ($\sim D_0$) increases with the fourth power of this spacing[15] (and consequently overweights the larger spacings), it is desirable to obtain a more accurate value of D_0. By noting that an element of the craze fibril having a diameter D can be envisioned to form through the uniaxial extension of a "phantom" isotropic element having a diameter D_0, then (cf. Figure 1C) D_0 must also be the fibril spacing within the mature craze. From geometric considerations it can be seen that for constant volume plastic deformation D and D_0 are related by

$$D_0 = \lambda_{craze}^{1/2} D \tag{4}$$

where λ_{craze} ($=1/v_f$) is the craze fibril extension ratio. From the values of λ_{craze} given in Table I, a plot of D_0 versus ν_e is shown in Figure 7. Clearly the dependence of D_0 on ν_e mirrors the dependence of $1/s_{max}$ on ν_e; however, the values of D_0 are consistently smaller than $1/s_{max}$ over the entire range.

The degree of splaying within the LAED pattern (i.e., the angular distribution of the scattered intensity along s_y) may be quantitatively characterized by plotting $i(s_y)$ at $s_x = s_{max}$. Displayed in Figure 8 is such a plot for the LAED pattern shown in Figure 1B. Indicated on this plot is the angle φ, which corresponds to the distance between the peak-to-peak positions in intensity along s_y. It should be pointed out that for some of the LAED patterns recorded it was not possible to fully resolve two individual peaks in $i(s_y)$; however, even under these conditions it may be seen that $\varphi > 0$. In this case two overlapping Gaussian curves were (summed and) forced to fit to the measured

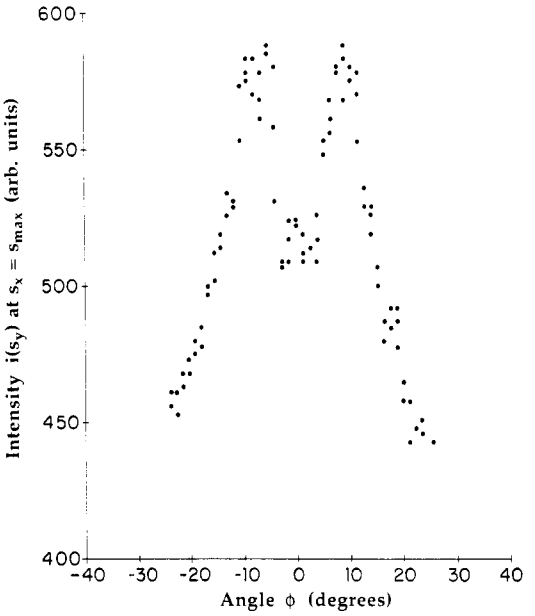

Figure 8. Plot of the angular separation $i(s_y)$ at $s_x = s_{max}$ for the LAED pattern (of a PMMA craze) shown in Figure 1B.

intensity profile, and the two peak positions were extracted from the centroid-to-centroid distance in this fit.[13,14] An example of such a fit, for a PαMS sample, is shown in Figure 9. Summarized in Figure 10 is the dependence of φ on ν_e, for all of the polymers examined. This plot clearly shows that φ increases almost linearly with increasing ν_e from $\varphi = 13.5°$ for the polymer examined with the lowest ν_e (i.e., PS) up to $\varphi \sim 20°$ for the polymer with the highest ν_e.

Discussion

As demonstrated in the preceding section, LAED is a powerful probe for examining the microstructure of crazes grown in a variety of polymer glasses. In particular the dependence of the craze microstructural parameters on the molecular entanglement density ν_e may be systematically studied for crazes produced at a homologous temperature ($T - T_g = -75$ °C) and strain rate. Moreover, the empirically determined scaling of D and D_0 with ν_e, reported here, may be compared to some recent models that describe the mechanism of craze fibril growth.

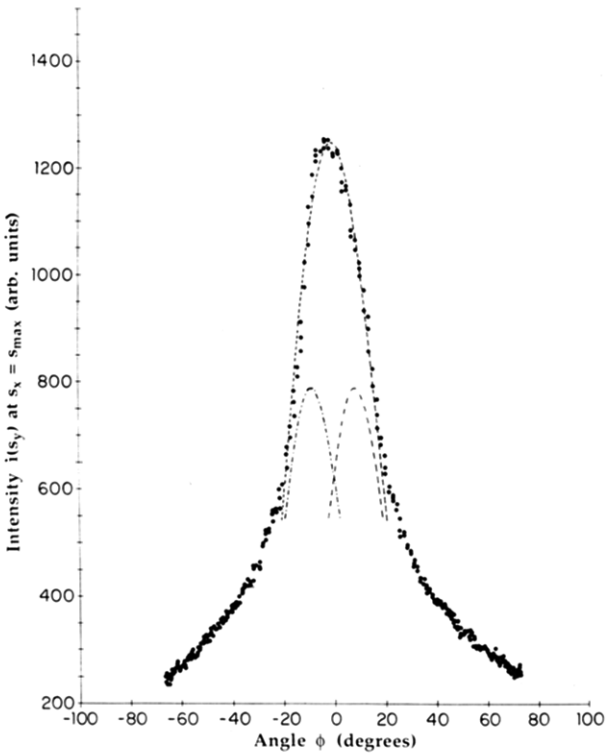

Figure 9. Two overlapping Gaussian curves forced to fit the measured intensity $i(s_y)$ profile (at $s_x = s_{max}$) for a PαMS sample. φ is determined from the centroid-to-centroid distance.

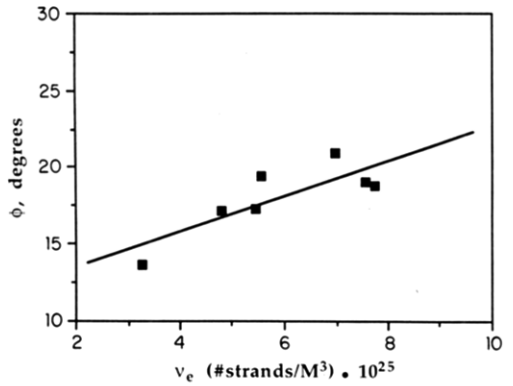

Figure 10. Plot of the angular separation φ versus entanglement density ν_e for crazes grown at $T - T_g = -75$ °C.

In one approach,[19,20] based on the Taylor meniscus instability model,[25-27] as the craze widens via a surface-drawing mechanism, the strain-softened polymer layer at the craze/bulk interface is transformed into a (highly oriented) fibril and void array. The geometry of this interface and the location of the strain softened region (the so-called active zone) are shown schematically in Figure 11.

This polymer layer may be modeled as a non-Newtonian fluid with the following flow law:

$$\sigma = \sigma_y(\dot{\epsilon}/\dot{\epsilon}_y)^{1/n} \tag{5}$$

where σ and $\dot{\epsilon}$ are the equivalent stress and strain rate in tension and σ_y, $\dot{\epsilon}_y$, and n are material parameters. (For large n, as is usually the case for glassy polymers, σ_y may be considered to be the flow stress of the fluid at a strain rate of $\dot{\epsilon}_y$.) Now, since the propagation of this fluid is driven by the gradient of the hydrostatic stress $|\nabla\sigma_0|$ (to the power n, where $n \approx 20$–30) at this boundary,[28] it is argued that the fibril spacing that maximizes this gradient will be the one observed. (It can easily be shown that even

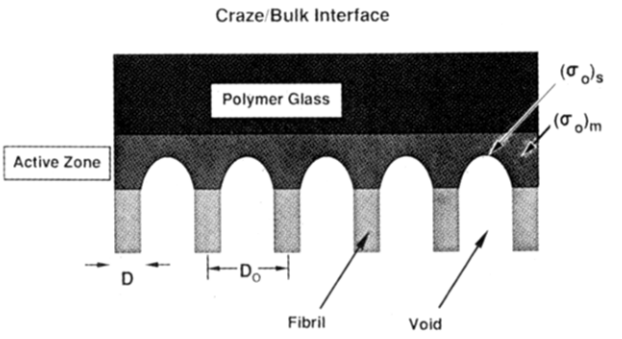

Figure 11.

small deviations from the value of D_0 that maximizes $\nabla\sigma_0$ result in an interface that advances at a significantly slower rate.) These assumptions lead to the prediction that the scale of fibrillation within the craze is governed by the product of the craze surface energy Γ and the reciprocal of the crazing stress S_c, viz.

$$D_0 \cong 8\Gamma/S_c \tag{6}$$

In turn the total craze surface energy Γ may be written as the sum of two terms, viz.

$$\Gamma = \gamma_s + \tfrac{1}{4}d\nu_e U_b \tag{7}$$

where the first term, γ_s, is the van der Waals *inter*molecular separation energy and the second term is the *intra*molecular bond breakage contribution where d is the root-mean-square end-to-end distance of an entangled strand (with mass M_e, the entanglement molecular weight) and U_b is the bond dissociation energy along the polymer backbone. Following Kramer,[19,20] the average tensile stress on the craze interface may be written as

$$S_c \propto (\sigma_y\Gamma/h)^{1/2} \tag{8}$$

where h is the thickness of the strain-softened polymer layer at the craze–bulk interface. By combining eq 6 and 8, one obtains the following expression:

$$D_0 \propto (\Gamma h/\sigma_y)^{1/2} \tag{9}$$

Since for polymer glasses σ_y scales as $(T - T_g)$,[29,30] noting that the product $d\nu_e$ (in eq 7) scales as $(\nu_e)^{1/2}$, eq 9 may be recast in the following form:

$$(D_0)_{T-T_g=\text{constant}} \propto h^{1/2}\nu_e^{1/4} \tag{10}$$

Therefore, a critical test of this prediction requires a knowledge of h for all the polymer glasses examined. Currently, however, there exists only limited information on the value h from polymer to polymer,[14] and thus a strictly quantitative comparison (between eq 10 and the data shown in Figure 7) is not possible. Nevertheless, if one makes the reasonable approximation[31] that, at a constant $T - T_g$ ($\cong$–75 °C), $h^{1/2}$ is roughly constant, then one obtains the following expression:

$$(D_0)_{T-T_g=\text{constant}} \propto \nu_e^{1/4} \tag{11}$$

This predicted scaling of D_0 with ν_e is shown by a dashed line in Figure 7, where it may be seen, in light of these simplifying assumptions, that the agreement between theory and experiment is qualitatively satisfactory.

It is evident from Figure 6 that the craze fibril diameter D also increases with increasing ν_e. The model of craze growth described above may also be used to predict the scaling of D with ν_e. By combining eq 4 and 11 and noting that $\lambda \propto \lambda_{Net}$ ($\propto \nu_e^{-1/2}$),[2,3] it can be shown that

$$(D)_{T-T_g=\text{constant}} \propto \nu_e^{1/2} \tag{12}$$

This predicted dependence of D on ν_e is illustrated by a dashed line in Figure 6. Here again the empirically determined scaling of D with ν_e is found to be in satisfactory qualitative agreement with the prediction. It should be pointed out that the prediction that D depends more strongly on ν_e than does D_0 (on ν_e) is consistent with the data. More importantly, however, it should be emphasized that independent of the model used to predict this scaling, both D and D_0 are found to increase only modestly with ν_e.

In addition to the main fibrils, transmission electron microscopy reveals the existence of a quasi-regular array of cross-tie fibrils[13,32,33] (cf. Figure 1A) whose dominant direction lies roughly parallel to the craze-bulk interface. The cross-tie fibrils bridge and pull the main fibrils away from the tensile axis $(\pm\varphi/2)°$ and consequently produce two preferred main fibril orientations, illustrated schematically in Figure 1B. Moreover, as a result of these two distinct orientations, the LAED patterns exhibit a splaying (cf. Figure 2A) that reflects the distribution of angular intensity along s_y.

Recently it was shown that cross-tie fibrils are produced during the surface drawing process of craze fibrillation.[13,14] In the model of craze growth briefly outlined above, it was tacitly assumed that entangled polymer strands that span two main fibrils must be lost during fibrillation. This assumption, however, is an oversimplification. Occasionally as the strain-softened region at the craze boundary (the active zone) propagates into the isotropic glass, entangled strands that bridge nearest-neighbor main fibrils will be pushed ahead of this interface and pile up locally. Subsequently, these local "pile-ups" of elastically strained entanglements will be drawn into the craze. At this point the strands can relax and, in doing so, pull the main fibrils away from the tensile axis $(\pm\varphi/2)°$. Therefore the microstructure of a "mature" craze consists of both main fibrils and a quasi-regular array of cross-tie fibrils. Apparently it is energetically more favorable for these local "pile-ups" to be integrated into the craze rather than to either break or disentangle them. Logically it may be expected that the likelihood of entangled strands bridging adjacent main fibrils would increase with increasing ν_e; accordingly φ should reflect this increase. The data displayed in Figure 10 are in agreement with this prediction.

Last, it should be noted that the dependence of the craze microstructural parameters on ν_e has a direct consequence on the craze fibril strength. In particular, as will be discussed in a subsequent publication,[18] the scale of D_0 controls the number of effectively entangled strands n_e that survive craze fibrillation. In turn the average force per n_e is believed to play a significant role in governing craze fibril stability.[5,6,18] The apparent link between craze strength and n_e provides important insight on the complex molecular and microscopic process of craze fibril breakdown.

Conclusions

The relationship between the craze microstructure and the molecular entanglement density ν_e, at a constant homologous $T - T_g = -75$ °C, for crazes grown in a series of glassy homopolymers, copolymers, and fully compatible polymer blends was determined. The values of the mean craze fibril diameter D and craze fibril spacing D_0 were observed to increase modestly with increasing ν_e. Moreover the empirical scaling of D and D_0 was found to be in satisfactory agreement with the meniscus instability model of craze growth. In addition the orientation φ of the fibril axis with respect to the tensile axis was observed to increase almost linearly with increasing ν_e; this increase reflects the increased contribution of the cross-tie fibrils in controlling the craze microstructure in high ν_e networks.

Acknowledgment. The careful experimental assistance of K. P. Leach is gratefully acknowledged.

Registry No. PMMA, 9011-14-7; PαMS, 25014-31-7; PSAN, 9003-54-7; PS, 9003-53-6; PO (SRU), 24938-67-8; PPO (homopolymer), 25134-01-4.

References and Notes

(1) Donald, A. M.; Kramer, E. J. *J. Polym. Sci., Part B: Polym. Phys.* **1982**, *20*, 899.
(2) Donald, A. M.; Kramer, E. J. *Polymer* **1982**, *23*, 461.
(3) Donald, A. M.; Kramer, E. J. *Polymer* **1982**, *23*, 1183.
(4) Henkee, C. S.; Kramer, E. J. *J. Polym. Sci., Part B: Polym. Phys.* **1984**, *22*, 721.
(5) Yang, A. C.-M.; Kramer, E. J.; Kuo, C. C.; Phoenix, S. L. *Macromolecules* **1986**, *19*, 2020.
(6) Yang, A. C.-M.; Kramer, E. J.; Kuo, C. C.; Phoenix, S. L. *Macromolecules* **1986**, *19*, 2010.
(7) Berger, L. L.; Kramer, E. J. *J. Mater. Sci.* **1987**, *22*, 2739.
(8) Henkee, C. S.; Kramer, E. J. *J. Mater. Sci.* **1986**, *21*, 1398.
(9) Berger, L. L.; Kramer, E. J. *Macromolecules* **1987**, *20*, 1980.
(10) Brown, H. R. *J. Polym. Sci., Part B: Polym. Phys.* **1983**, *21*, 483.
(11) Yang, A. C.-M.; Kramer, E. J. *J. Polym. Sci., Part B: Polym. Phys.* **1985**, *23*, 1353.
(12) Berger, L. L.; Buckley, D. J.; Kramer, E. J.; Brown, H. R.; Bubeck, R. A. *J. Polym. Sci., Part B: Polym. Phys.* **1987**, *25*, 1679.
(13) Miller, P.; Kramer, E. J. Deformation, Yield and Fracture of Polymers. *Proc. Plastics Rubber Inst. Conf.* **1988**, *81/1*; Churchill College: Cambridge, U. K.
(14) Miller, P. Ph.D. Thesis, Cornell University, Ithaca, NY, 1987.
(15) Brown, H. R.; Kramer, E. J. *J. Polym. Sci., Part B: Polym. Phys.* **1981**, *19*, 487.
(16) Paredes, E.; Fischer, E. *Makromol. Chem.* **1979**, *180*, 2707.
(17) Westbrook, P. A.; Fellers, J. F.; Hendricks, R. W.; Lin, S. J. *J. Polym. Sci., Part B: Polym. Phys.* **1983**, *21*, 969.
(18) Berger, L. L., to be published.
(19) Kramer, E. J. *Polym. Engr. Sci.* **1984**, *24*, 761.
(20) Kramer, E. J. *Adv. Polym. Sci.* **1983**, *52/53*, 1.
(21) Lauterwasser, B. D. Ph.D. Thesis, Cornell University, Ithaca, NY, 1979.
(22) This vertical (refraction) streak completely vanishes for LAED patterns taken from wide crazes that are placed wholly within the objective aperture.
(23) Porod, G. *Kolloid Z.* **1951**, *124*, 83; *Ibid.* **1952**, *125*, 109.
(24) To obtain an accurate value of Q, it is necessary to evaluate this integral to infinite s by using Porod's law, i.e., $Q = 2\pi\int_0^{s_p} si(s)\,ds + 2\pi k_1/s_p$, where s_p is in the region of s where $i(s) = k_1/s^3$.
(25) Taylor, G. I. *Proc. R. Soc.* **1950**, *A210*, 192.
(26) Fields, R. J.; Ashby, M. F. *Philos. Mag.* **1976**, *33*, 33.
(27) Argon, A. S.; Salama, M. M. *Philos. Mag.* **1977**, *36*, 1217.
(28) As shown in Figure 11, the gradient $\nabla\sigma_0$ can be approximated by $2[(\sigma_0)_m - (\sigma_0)_s]/D_0$, where $(\sigma_0)_m$ and $(\sigma_0)_s$ are the hydrostatic tensions in the active zone at a position directly above the fibril and at the surface of the void ceiling between the fibrils, respectively. In turn $(\sigma_0)_m$ is proportional to the average tensile stress on the craze interface, and $(\sigma_0)_s$ is given by capillarity (i.e., $\cong 4\Gamma/D_0$).
(29) Kambour, R. P. In *Mechanisms of Environmental-Sensitive Cracking of Materials*; Swann, P. R., Ford, F. P., Westwood, A. R. C., Eds.; Materials Society; London, 1977; p 213.
(30) Haward, R. N.; Murphy, B. M.; White, E. T. F. *J. Polym. Sci., Part A* **1971**, *29*, 801.
(31) Since the scale of h is determined by the extent of strain softening (and hence strain localization) at the craze boundary, this value is not expected to be strongly dependent on ν_e. However, the width of h is known to increase with increasing $T - T_g$ (see ref 14).
(32) Beahan, P.; Bevis, M.; Hull, D. *J. Mater. Sci.* **1972**, *8*, 162.
(33) Beahan, P.; Bevis, M.; Hull, D. *Philos. Mag.* **1971**, *24*, 1267.